Effect of free-carrier absorption on the threshold current density of GaAs/(Al,Ga)As quantum-cascade lasers

M. Giehler,[a] H. Kostial, R. Hey, and H. T. Grahn
Paul-Drude-Institut für Festkörperelektronik, Hausvogteiplatz 5-7, 10117 Berlin, Germany

(Received 15 March 2004; accepted 11 August 2004)

$GaAs/Al_{0.33}Ga_{0.67}As$ quantum-cascade lasers with plasmon-assisted waveguides exhibit a decreasing threshold current density j_{th} with increasing wave number ν_0 of the laser line, which changes as a function of the injector doping density. We have developed an analytical approach based on the effective dielectric tensor component for the *p*-polarized light emitted from a quantum-cascade laser, which explains the observed dependence of $j_{th}(\nu_0)$ in terms of losses due to free-carrier absorption predominantly in the doped waveguides $\alpha_{WG}(\nu_0)$. A contribution to the losses by free-carrier absorption in the quantum-cascade structure itself and subsequently to j_{th} can be neglected except for very high injector doping densities. The calculated values for $\alpha_{WG}(\nu_0)$ are in good agreement with the experimental data. Our approach quantitatively predicts the observed decrease of j_{th} from 17 to 7 kA cm^{-2} with increasing ν_0 between 900 and 1100 cm^{-1}. In addition to achieving a direct physical insight into the influence of free-carrier absorption on the laser performance, the proposed analytical approach provides a simple tool for the determination of the waveguide losses for any quantum-cascade laser without adopting a numerical solver. © *2004 American Institute of Physics*. [DOI: 10.1063/1.1803635]

I. INTRODUCTION

$GaAs/Al_{0.33}Ga_{0.67}As$ quantum-cascade lasers (QCLs) were first introduced by Sirtori *et al.*[1] Their performance was greatly improved by replacing the $Al_{0.9}Ga_{0.1}As$ waveguides (WGs) by plasmon-assisted ones,[2] which possess much better electrical properties, but, at the same time, increased optical losses. Recently, we have investigated the lasing properties of $GaAs/Al_{0.33}Ga_{0.67}As$ QCLs as a function of the injector doping density expressed in terms of the sheet carrier concentration n_s per period.[3] We found that intermediately doped QCLs with $n_s \approx 6\times10^{11}$ cm^{-2} exhibit a maximum in the wave number ν_0 of the laser line and, at the same time, a minimum in the threshold current density j_{th}.[3] For lower and higher doping densities, j_{th} decreases almost linearly with increasing ν_0 as shown in Fig. 1. Since we investigated seven different doping densities and for the lowest doping density three QCLs, a total of nine data points is shown in Fig. 1.

In order to explain this dependence of $j_{th}(\nu_0)$, we report in this paper an investigation of the influence of the free-carrier absorption (FCA) on the optical losses and subsequently on j_{th} for $GaAs/Al_{0.33}Ga_{0.67}As$ QCLs with plasmon-assisted WGs. In contrast to all other investigations, which use a numerical solver for the calculation of the optical losses in the resonator, we treat the effect of FCA on the optical losses using an analytical approach. In this way, we also obtain a better physical insight into the influence of FCA on the WG losses. Finally, we compare our calculated data for the optical losses through FCA and its influence on j_{th} with experimental data for a weakly as well as an intermediately doped two-sectioned QCL.

[a]Author to whom correspondence should be addressed; electronic mail: giehler@pdi-berlin.de

II. SAMPLES

The QCLs were grown by molecular-beam epitaxy (MBE) with 30 periods for the cascade structure. The layer sequence of all $GaAs/Al_{0.33}Ga_{0.67}As$ cascade structures used in this study is nominally the same as introduced by Sirtori *et al.*[1] However, the Si concentration in the four doped injector layers was varied resulting in sheet carrier densities between 3.5×10^{11} and 1.0×10^{12} cm^{-2} per period,[3] which correspond to averaged bulk concentrations n between 3.7 and 10.7 $\times10^{17}$ cm^{-3} using the total thickness of 9.4 nm for these four doped layers. The sheet carrier concentration was determined by capacitance-voltage measurements on step-etched pieces showing good agreement with the nominal values. All

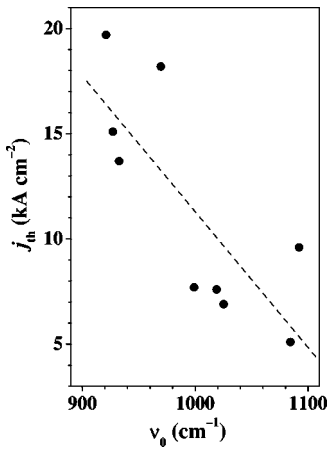

FIG. 1. Measured threshold current density j_{th} vs wave number ν_0 of the laser lines for $GaAs/Al_{0.33}Ga_{0.67}As$ QCLs with plasmon-assisted WGs at 8 K. Note that we investigated seven QCLs with different doping densities as well as three QCLs with the same doping density in the injector resulting in a total of nine data points. Most of the data are taken from Ref. 3. The dashed line indicates a linear fit to the data points.

QCL structures were characterized by double-crystal x-ray diffraction measurements to demonstrate that the actual layer thicknesses as well as the Al content agree within 2% with the nominal values.

We used plasmon-assisted WGs on the top and bottom of the active zone of each QCL following Ref. 2. Each WG consists of a 4 μm thick, weakly doped GaAs layer with a doping concentration $n=4\times10^{16}$ cm^{-3} and a 1 μm thick, strongly doped GaAs layer, in which we have reduced the doping density from $n^+=6\times10^{18}$ cm^{-3} in Ref. 2 to $n^+=4\times10^{18}$ cm^{-3}.

The laser stripes with typical dimensions of 19×2400 μm^2 were prepared by plasma etching, where the side walls of the lasers were defined by 7 μm deep and 2.5 μm broad trenches refilled by a photoresist. The laser emission was studied using pulse-mode operation with a width of 100 ns and a repetition rate of 5 kHz at 8 K. The infrared spectra were recorded using a Fourier-transform spectrometer with a spectral resolution of 0.12 cm^{-1}. The QCLs were mounted with the substrate on a cold finger in a He-flow cryostat without exchange gas and heat management. Therefore, heating of the laser stripe is expected during the current pulse.

III. CARRIER DENSITY DEPENDENCE OF THE FREE-CARRIER ABSORPTION COEFFICIENT IN *n*-TYPE GaAs

In order to obtain an analytical relation between j_{th} and n or ν_0, we first need to investigate FCA in differently doped GaAs layers, since the doping density in the cascade structure differs from the one in the WGs. Therefore, we have measured the infrared reflectance and transmittance spectra of bulk *n*-type GaAs samples as well as MBE-grown layers in the spectral region between $\nu=500$ and 2500 cm^{-1}. The reflectance spectra are mainly determined by the real part of the dielectric function (DF) ϵ, i.e., Re$\{\epsilon\}$. The contribution of the free carriers to Re$\{\epsilon\}$ is well described by the classical Drude model. Therefore, the reflectance spectra can be reproduced by using a DF consisting of a harmonic-oscillator phonon contribution as well as a free-carrier Drude term, where the density n and the averaged energy-independent scattering rate γ of the free carriers were used as fit parameters. γ is related to the mobility μ by $\mu=e/(m^*\gamma)$. For the different samples, the obtained values for n vary between 1.1×10^{17} and 2.6×10^{18} cm^{-3}, while μ lies between 4000 and 900 cm^2/(V s). The values for both quantities agree well with the ones obtained from electrical measurements.

For the determination of the FCA coefficient $\alpha_{\mathrm{FC}}(\nu,n)$, we have measured transmittance spectra at room temperature and at 77 K. In contrast to the reflectance spectra, the absorption coefficient is essentially determined by the imaginary part of the DF ϵ, i.e., Im$\{\epsilon\}$, which depends on the dominant scattering mechanism of the free carriers. For scattering of free carriers on acoustical (ac) and longitudinal optical phonons (op) as well as ionized impurities (imp), the following relation is approximately valid in the high-frequency limit,[4,5] i.e., $\hbar\omega>E_F$, where E_F denotes the Fermi energy of the free carriers, and $\omega/\gamma\gg1$

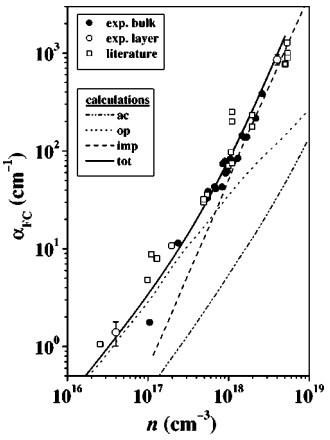

FIG. 2. FCA coefficient $\alpha_{\mathrm{FC}}(\tilde{\nu})$ vs carrier concentration n measured at $\tilde{\nu}=1000$ cm^{-1} and 300 K for *n*-type GaAs samples. The dots indicate our experimental data on bulk GaAs crystals, the circles experimental data of *n*-type GaAs layers on SI-GaAs, and the open squares data from the literature (Refs. 6–8). The calculated contributions of the different scattering mechanisms are shown as a dashed-dotted line for acoustic phonons (ac), dotted line for longitudinal optical phonons (op), and dashed line for ionized impurities (imp). The solid line (total) indicates the calculated data for the total $\alpha_{\mathrm{FC}}(\tilde{\nu},n)$ according to Eq. (3).

$$\alpha_{\mathrm{FC}}(\nu,n,\theta)\approx c_{\mathrm{ac}}n\nu^{-1.5}+c_{\mathrm{op}}n\nu^{-2.5}+c_{\mathrm{imp}}n^2\frac{1+\theta(n)}{1-\theta(n)}\nu^{-3.5}, \tag{1}$$

where $\theta=N_A^-/N_D^+$ denotes the compensation ratio of the ionized impurities. The coefficients c_i (i=ac, op, imp) for *n*-type GaAs were calculated in Refs. 4 and 5. Both datasets almost agree with each other at room temperature. Using the values given for the coefficients c_i in Ref. 5 and the values of n determined from the reflectance spectra, the absorption spectra of the *n*-type GaAs samples for n between 4×10^{16} and 4×10^{18} cm^{-3} and wave numbers ν between 800 and 1500 cm^{-1} can be well described by

$$\alpha_{\mathrm{FC}}(\nu,n)\approx\alpha_{\mathrm{FC}}(\tilde{\nu},n)\left(\frac{\nu}{\tilde{\nu}}\right)^{-r(n)}, \tag{2}$$

where $\tilde{\nu}=1000$ cm^{-1} and $r(n)=2.5$, 2.9, and 3.35 for $n\approx4\times10^{16}$, 4×10^{17}, and 4×10^{18} cm^{-3}, respectively. In Eq. (2), a compensation ratio $\overline{\theta(n)}$ has been included, which was averaged over all samples with comparable n. From the measured data, we estimate an uncertainty of $\Delta\alpha_{\mathrm{FC}}(\tilde{\nu},n)=\pm20\%$ and of $\Delta r(n)=\pm0.1$, predominantly due to the deviation of the compensation ratio from its average value. The different values of r indicate that the interaction of free carriers with longitudinal optical phonons dominates for weak and intermediate doping densities, while the contribution of free-carrier scattering on ionized impurities becomes the most important one for strong doping densities resulting in almost temperature independent absorption spectra. The significant deviation of r from the value 2 predicted by the Drude formula indicates that the Drude model cannot be applied to estimate the carrier density and wave number dependence of the FCA in *n*-type GaAs, because the energy dependence of the free-carrier scattering processes has been neglected.

Figure 2 shows the measured values (dots) of $\alpha_{FC}(\tilde{\nu})$ versus n for bulk, n-type GaAs samples obtained at 300 K. Our measured values are in good agreement with published data[6–8] indicated by the open squares in Fig. 2. The scatter of our experimental values and the data in the literature is mainly due to different compensation ratios in the various samples. Furthermore, Fig. 2 also shows $\alpha_{FC}(\tilde{\nu},n)$ for the three different scattering mechanisms ac, op, and imp calculated using the exact theory described in Ref. 5 and the experimental values for n and $\overline{\theta}(n)$ obtained from the fits of the reflectance and absorption spectra. The solid line in Fig. 2 demonstrates that the dependence of our experimentally determined values for $\alpha_{FC}(\tilde{\nu},n)$ can be well approximated by

$$\alpha_{FC}(\tilde{\nu},n) \approx c_1 n + c_2 n^2 + c_3 n^3, \tag{3}$$

where $c_1 = 2.9 \times 10^{-17}$ cm^2, $c_2 = 5.1 \times 10^{-35}$ cm^5, and $c_3 = 5.1 \times 10^{-55}$ cm^8. In Eq. (3), the first term, which is linear in n, describes the dependence of the interaction of free carriers with phonons, whereas the quadratic term in n reflects the scattering of free carriers on ionized impurities in uncompensated samples. Depending on the actual element used for doping, the prefactor $[1+\overline{\theta}(n)]/[1-\overline{\theta}(n)]$ in Eq. (1) increases, in particular, for higher doping concentrations, with increasing n, which leads to the cubic term in Eq. (3). However, the contribution of this cubic term is always rather small, e.g., for $n = 4 \times 10^{18}$ cm^{-3}, it only accounts for 4% of the contribution of the second term.

In order to test, if the data for $\alpha_{FC}(\tilde{\nu},n)$ of MBE-grown layers agree with the ones of bulk crystals, we have also measured transmittance spectra of a weakly doped and a strongly doped GaAs layer with a thickness of 8 and 2 μm, respectively, grown on SI-GaAs. For the weakly doped layer, the nominal doping density of $n = 4 \times 10^{16}$ cm^{-3} corresponds to the one in the layer separating the cascade from the plasmon WG layer in our QCLs, while the nominal concentration of $n^+ = 4 \times 10^{18}$ cm^{-3} in the strongly doped layer was set equal to the one in the plasmon WG layer in our QCLs. In order to precisely determine $\alpha_{FC}(\nu,n)$ from the transmittance spectra of thin layers grown on a substrate, we have to suppress any changes of the transmittance due to light scattering caused by the unpolished back side of the substrate. Hence, we used substrates, which were polished on both sides. In the interferogram, the secondary peak due to the internal reflections within the sample was replaced by a straight line, which corresponds to a spectral averaging of the intensities. This incoherent averaging was taken into account in the determination of $\alpha_{FC}(\nu,n)$ from the measured reflectance and transmittance spectra according to Ref. 9. The values obtained for $\alpha_{FC}(\tilde{\nu},n)$ for the weakly and strongly doped layers are also included in Fig. 2 as circles. These data agree well with the ones of bulk crystals indicating that Eqs. (2) and (3) can also be applied to n-type GaAs layers with concentrations between 4×10^{16} and 4×10^{18} cm^{-3}, in particular, for the plasmon-assisted WG layers in our QCLs.

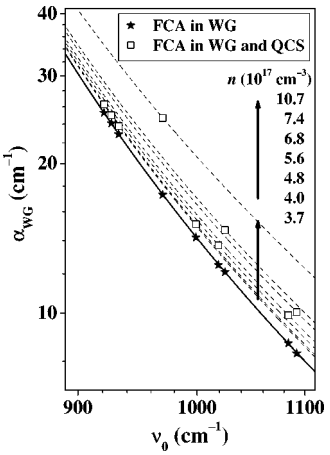

FIG. 3. Calculated WG losses α_{WG} due to FCA at low temperatures vs ν_0 in a double logarithmic representation. The solid line indicates the result taking into account only the top and bottom WGs with the stars marking the positions of the laser lines. The dashed lines indicate the results taking into account the WGs and the cascade for different doping densities as indicated by the open squares marking the positions of the laser lines.

IV. CALCULATION OF THE WAVEGUIDE LOSSES IN A QCL DUE TO FREE-CARRIER ABSORPTION

For the determination of the WG losses $\alpha_{WG}(\nu)$ in QCLs, which emit p-polarized light along the plane of the layers, we have to calculate the in-plane component of the dielectric tensor ε, which according to Ref. 10 is given by

$$\varepsilon_{\parallel}^{-1}(\nu) = \frac{1}{\sum_l (\Gamma_l d_l)} \left(\sum_l \frac{\Gamma_l d_l}{\epsilon_l(\nu,n)} \right). \tag{4}$$

Here ϵ_l and d_l denote the complex DF and thickness, respectively, of the lth layer in the QCL. Γ_l refers to the overlap factor of the lth layer with the laser mode, i.e., it denotes the ratio of the energy of the laser mode stored in the lth layer and the total energy of the laser mode. We assume $\Gamma_l = 1$ for all layers except for the WG layers with $n^+ = 4 \times 10^{18}$ cm^{-3}. Furthermore, in order to derive Eq. (4), it has been assumed that $n_{opt,l}\, d_l \ll 1/\nu$, where $n_{opt,l}$ denotes the refractive index of the lth layer. The values of $\mathrm{Re}\{\epsilon_l\}$ and $n_{opt,l}$ were mainly obtained from the reflectance spectra, whereas $\mathrm{Im}\{\epsilon_l(\nu,n)\} = n_{opt,l}\alpha_{FC,l}(\nu,n)/(2\pi\nu)$ was predominantly determined from the absorption spectra according to Eq. (1) using $\theta = \overline{\theta}(n)$ as discussed in connection with Eq. (2). After using Eq. (4) to determine $\varepsilon_{\parallel}^{-1}(\nu)$ by summing over all layers in the complete QCL structure, the WG losses $\alpha_{WG}(\nu)$ are calculated according to $\alpha_{WG}(\nu) = 2\pi\nu\, \mathrm{Im}\{\varepsilon_{\parallel}(\nu)\}/n_{opt}$, where $n_{opt} \approx \sqrt{\mathrm{Re}\{\varepsilon_{\parallel}\}}$.

Figure 3 shows the calculated values of α_{WG} versus ν_0 for our QCLs, which lase at different wave numbers ν_0,[3] in a double logarithmic representation. In order to demonstrate the influence of the FCA on α_{WG}, we neglect in the calculation any wave number dependence of the optical confinement and set $\Gamma_{WG(n^+)} = 0.018$. Near $\tilde{\nu} = 1000$ cm^{-1}, the refractive index $n_{opt,WG(n^+)}(\nu)$ of the WG(n^+) layers is approximately given by $\sqrt{\mathrm{Re}\{\varepsilon_{WG(n^+)}(\nu)\}}$, where $\varepsilon_{WG(n^+)}(\nu) = 5.77(\nu/\tilde{\nu})^{2.2} + i0.51(\nu/\tilde{\nu})^{-4.35}$. Therefore, $n_{opt,WG(n^+)}(\nu)$ increases with increasing ν and eventually approaches the values of $n_{opt,l}$ of the surrounding weakly doped WG layer and

the layers in the cascade. This effect alone would result in a decreasing optical confinement of the laser mode. However, this decrease is partially compensated by the typically increasing confinement with increasing ν. Therefore, the approximation of a constant value for $\Gamma_{\mathrm{WG}(n^+)}$ is justified.

The solid line in Fig. 3 indicates the values of α_{WG} assuming that only FCA in the top and bottom WGs contributes to the optical losses. The stars mark the wave numbers of the measured laser lines. Figure 3 demonstrates that $\alpha_{\mathrm{WG}}(\nu_0)$ strongly decreases with increasing ν_0. It can be approximately described by the power law $\alpha_{\mathrm{WG}}(\nu_0) \approx 15(\nu_0/\tilde{\nu})^{-6.6}$. The rather large absolute value of the exponent originates from the very different exponents of the wave number dependence of the real and imaginary part of the DF of the strongly doped WG layers as described in the previous paragraph in comparison to the undoped layers in the cascade, which are coupled in a nonlinear fashion according to Eq. (4).

In addition to the doped WGs, also the four doped layers inside each period of the cascade structure may contribute to FCA. While free carriers in quantum wells are free to move in the plane of the layers, they are confined along the growth direction. Because in a QCL the electric field of the laser light is polarized parallel to the growth direction, the FCA is modified.[11] Furthermore, interface roughness enables additional scattering events even for *p*-polarized light.[12] In order to estimate the upper limit of the modified FCA in the cascade, we assume that all four doped layers in each period contribute to the optical losses in the same way as FCA in thick GaAs layers. Using this approximation, we determine the maximum value of the optical losses due to FCA in the WGs and in the cascade for the seven different doping densities in the injector of our QCLs, which are indicated by the dashed lines in Fig. 3. Note that according to Eq. (4) α_{WG} nonlinearly increases with increasing doping density in the injectors of the QCLs as indicated by the arrow. Furthermore, with increasing doping density in the cascade, the exponent of the power law for $\alpha_{\mathrm{WG}}(\nu_0)$ slightly decreases. We conclude that the optical losses due to FCA in a QCL are mainly determined by FCA in the waveguide. Only for injector doping concentrations above 7.5×10^{17} cm^{-3}, the cascade itself notably contributes to the optical losses due to FCA.

V. INFLUENCE OF THE WAVEGUIDE LOSSES ON THE THRESHOLD CURRENT DENSITY OF QCLS

We now determine the influence of the WG losses on the threshold current density. This dependence is described by

$$j_{\mathrm{th}}(\nu_0) = \frac{\alpha_{\mathrm{WG}}(\nu_0) + \alpha_M}{g\Gamma}, \tag{5}$$

where $\alpha_M = -(1/L)\ln(1/R) = 5.3$ cm^{-1} denotes the mirror losses for a GaAs-based QCL of 2.4 mm length, g the gain coefficient, and Γ the overlap factor of the laser mode with the gain medium. Following Ref. 2, we assume $\Gamma = 0.31$, i.e., 31% of the energy of the laser mode is stored in the gain medium, which for QCLs is approximated by the whole cascade structure. Consequently, 67% of the energy of the laser mode is leaking into the weakly doped WG layers, which are located between the WG(n^+) layers with $\Gamma_{\mathrm{WG}(n^+)} \approx 2\%$ and the cascade structure. The solid line and the stars in Fig. 4 indicate the best fit to the experimental data (dots) for $j_{\mathrm{th}}(\nu_0)$ taking into account FCA in the WGs alone, resulting in a value for the wave-number-independent gain coefficient of $g_a = 6.60$ cm kA^{-1} with a standard deviation of 1.63 cm kA^{-1}. The wave number dependence of the FCA in the WGs alone results in a decrease of j_{th} from 17 to 7 cm kA^{-1} for QCLs with an increasing lasing energy between 900 and 1100 cm^{-1}. Figure 4 also shows that, when the additional contribution to the optical losses by FCA in the cascade itself is taken into account, the agreement between the calculated (open squares) and measured (dots) j_{th} is slightly improved as demonstrated by the decrease of the relative standard deviation of the gain coefficient from 0.25 to 0.23. In this case, we obtain the best fit for a wave-number-independent gain coefficient $g_a = (7.20 \pm 1.68)$ cm kA^{-1}. Table I lists the calculated values of j_{th} for two reference QCLs, which will be used in the following section to determine the WG losses experimentally.

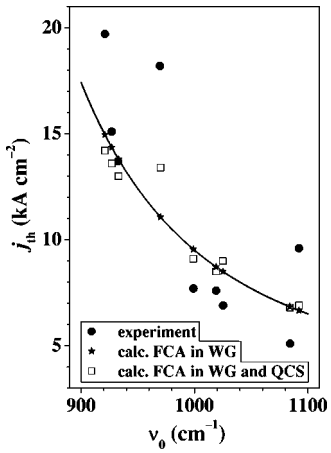

FIG. 4. Threshold current density j_{th} vs ν_0. The experimental data are indicated by dots, the solid line and the stars mark the calculated data taking into account FCA only in the WGs, and the open squares for FCA in the WGs and cascade structure.

VI. EXPERIMENTAL DETERMINATION OF THE WAVEGUIDE LOSSES IN TWO-SECTIONED QCLS

Since the condition $n_{\mathrm{opt},i}d_i \ll 1/\nu$ used in the derivation of Eq. (4) is not necessarily fulfilled for all layers within a QCL structure, we tested the validity of Eq. (4) for the calculation of $\alpha_{\mathrm{WG}}(\nu_0)$ using two specially prepared lasers DL1 and DL2, which consist of two-sectioned lasers. The laser DL1 (DL2) was weakly (intermediately) doped with $n = 3.7\times10^{17}$ cm^{-3} ($n = 4.8\times10^{17}$ cm^{-3}) as listed in Table I. The total length and width of the laser stripe was $L = 2.8$ mm (2.0 mm) and $w = 19$ μm (29 μm) for DL1 (DL2). Each DL consists of two sections, a front part (f) and a back part (b), where for both DLs the length of each section is given by $L_f \approx L/3$ and $L_b \approx 2L/3$. In order to prevent leakage currents between both parts, the two sections are separated by an air gap. This gap with a width of about 350 nm was produced by fixing the laser with the bottom contact on a metal plate and

TABLE I. Structure, doping density n, measured emission wave number ν_0, WG losses α_{WG}, and threshold current densities j_{th} of a weakly and an intermediately doped DL as well as data for the corresponding nonsectioned reference QCLs. For the determination of $\alpha_{WG}(\nu_0)$, we have used $g=7.2$ cm kA^{-1} and $\Gamma=0.31$.

			α_{WG} (cm^{-1})			j_{th}(kA cm^{-2})	
Structure	n (10^{17} cm^{-3})	ν_0 (cm^{-1})	Method I Eq. (7)	Method II Eq. (8)	calc.[a] Eq. (4)	expt.	calc.[a] Eq. (5)
DL1	3.7	965	13.1	21.9	18.8	10.1	10.8
QCL1	3.7	927[b]			25.0	16.2[b]	13.6
DL2	4.8	1017	11.4	12.9	13.8	9.1	8.5
QCL2	4.8	1019[b]			13.7	7.6[b]	8.5

[a]Assuming that FCA in all doped layers in the QCL contributes to α_{WG}.
[b]Data taken from Ref. 3.

carefully cleaving only the laser. The horizontal misalignment between the edges was less than 20 nm, and the longitudinal axes of both laser parts were tilted by less than 0.01° with respect to each other. The presence of the air gap in the laser stripe slightly modifies the resonator and consequently also the lasing properties of the DLs with respect to the corresponding reference QCLs studied previously.[3] First, the optical intensity is reduced due to reflections at the gap. From calculations as well as from intensity versus current measurements on QCLs with and without an air gap, we estimate that the optical attenuation due to this air gap is less than 10%. Therefore, it is much less than the optical losses due to FCA, and consequently we can neglect the influence of the air gap. Second, the lasing energy of the DLs is changed with respect to the corresponding reference QCLs mainly due to the modification of the resonator. Whereas the weakly and intermediately doped DLs show lasing at 965 and 1017 cm^{-1}, respectively, the values for the corresponding reference QCLs as listed in Table I are 927 and 1019 cm^{-1}, respectively.[3] Furthermore, the threshold current densities of the DLs, where j_{th} was measured with both parts of the DL being directly electrically connected, are also slightly changed with respect to values of the reference QCLs (cf. Table I). Note that for both DLs $j_{th}<(j_{th,f}+j_{th,b})$, where $j_{th,i}$ for $i=f$ and b denotes the threshold current density for the corresponding section i of the DL.

We have determined the WG losses in the two-sectioned QCLs in two different ways. In the first approach referred to as method I, the currents I_f and I_b through each section of the DL are measured at lasing threshold of the complete QCL. The corresponding threshold condition for the total optical WG losses $\alpha_t(\nu_0)$ can be written as[13]

$$\alpha_t(\nu_0)=\alpha_{WG}(\nu_0)+\alpha_M=G_{M,f}(j_f,\nu_0)\frac{L_f}{L}+G_{M,b}(j_b,\nu_0)\frac{L_b}{L}, \tag{6}$$

where $G_{M,i}=g\Gamma j_i$ denotes the modal gain and j_i the current density. Using Eq. (6) and $j_i=I_i/(wL_i)$, the threshold condition is related to I_f and I_b through

$$I_b=-I_f+\frac{\alpha_t(\nu_0)wL}{g\Gamma}=-I_f+C. \tag{7}$$

Figure 5 shows the measured currents I_b versus I_f at the lasing threshold for both DLs. Assuming a linear relation between I_b and I_f as suggested by Eq. (7), a linear fit of the measured data results in $I_b=-1.00I_f+4.36$ A for DL1 and $I_b=-0.82I_f+4.43$ A for DL2. Whereas the slope of I_b versus I_f for DL2 is somewhat smaller than the expected value of one, it is in excellent agreement with Eq. (7) for DL1. From the measured values of the constant C, we have determined $\alpha_{WG}(\nu_0)$ using Eqs. (6) and (7) by assuming a wave-number-independent gain coefficient $g_a=7.2$ cm kA^{-1} and $\Gamma=0.31$ as discussed in the preceding section. The obtained values for $\alpha_{WG}(\nu_0)$, which are listed in Table I, are clearly smaller than the calculated data taking into account FCA in the WGs and in the four doped layers of each period of the cascade structure (Sec. IV A).

The second method (method II) consists of measuring the intensities emitted from one part of the DL through both end facets. These measurements were carried out for current values up to slightly above the lasing threshold. From the intensity S_A emitted from the front part and the intensity S_B emitted from the back part measured under the condition that $I_f=0$ and $I_b>0$, we can obtain $\alpha_{WG}(\nu_0)$ from the equation

$$S_A\approx S_B\exp[-\alpha_{WG}(\nu_0)L_f]. \tag{8}$$

Note that these measurements can also be performed by exchanging the electrical injection conditions, i.e., $I_f>0$ and

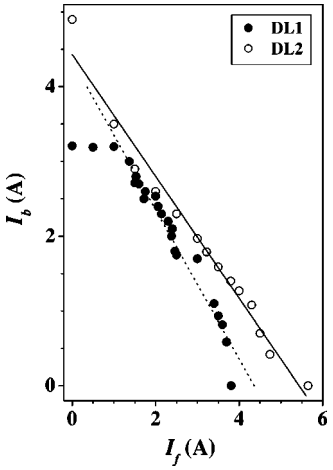

FIG. 5. Measured current I_b vs I_f at the lasing threshold for DL1 (dots) and DL2 (circles) at 8 K. The dashed and solid line indicate a linear fit of the respective dataset.

$I_b = 0$. The data determined by method II are also listed in Table I. The corresponding values are clearly larger than the ones determined by method I and will be discussed below.

VII. COMPARISON OF THE CALCULATED AND MEASURED WAVEGUIDE LOSSES AND THE RESULTING THRESHOLD CURRENT DENSITIES

First, we compare the calculated and measured data for the WG losses. Table I shows that the calculated values of $\alpha_{WG}(\nu_0)$ in Sec. IV agree well with the ones that were experimentally determined on DLs by method II, whereas the values obtained by method I are clearly too small. Our calculated and measured (method II) values of $\alpha_{WG}(\nu_0)$ agree quite well with calculated values published in the literature. Sirtori *et al.*[2] reported a calculated value of $\alpha_{WG}(\nu_0) = 16\ \mathrm{cm}^{-1}$ for a QCL with the same layer structure, an injector doping density between QCL1 and QCL2 in Table I, and a considerably higher doping density in the plasmon-assisted WGs using the parameters $\nu_0 = 1064\ \mathrm{cm}^{-1}$, $n^+ = 6 \times 10^{18}\ \mathrm{cm}^{-3}$, $\Gamma(n^+) = 0.008$, and $\Gamma = 0.31$. With our model, we obtain for a QCL with the same doping level in the plasmon-assisted WGs exactly the same value $\alpha_{WG}(\nu_0) = 16\ \mathrm{cm}^{-1}$, which justifies our approach, in particular the use of an effective dielectric tensor for the QCL structure [Eq. (4)]. However, a comparison of the experimental data for QCLs with different doping densities in the WGs is much more difficult. In Ref. 2, the experimental value of $\alpha_{WG}(1064\ \mathrm{cm}^{-1})$ is given as 19 and 21 cm^{-1} obtained with two different methods, while in Ref. 13 an experimental value of 22 cm^{-1} is reported. In contrast to these values, we would obtain $\alpha_{WG}(1064\ \mathrm{cm}^{-1}) \approx 9\ \mathrm{cm}^{-1}$ by extrapolating our values measured on the DLs by method II to the emission wave number $\nu_0 = 1064\ \mathrm{cm}^{-1}$, which is much smaller than the measured values in Refs. 2 and 13. Nevertheless, this difference does not invalidate our experimental data, since the doping level in the WGs is with $n^+ = 4 \times 10^{18}\ \mathrm{cm}^{-3}$ considerably lower than in Refs. 2 and 13. If we calculate the WG losses for a laser with $\nu_0 = 1064\ \mathrm{cm}^{-1}$ and a WG doping of $4 \times 10^{18}\ \mathrm{cm}^{-3}$, we obtain $\alpha_{WG}(1064\ \mathrm{cm}^{-1}) = 10.4\ \mathrm{cm}^{-1}$, which agrees quite well with the experimental, extrapolated value. We conclude that a comparison of experimental data obtained on QCLs with differently doped WGs supports our model.

Now we will compare the gain coefficient obtained from our measurements with values in the literature. From Eq. (5) in Sec. V, we obtained a wave-number-independent value $g_a = 7.2\ \mathrm{cm\,kA}^{-1}$ for our QCLs. According to Ref. 14, the gain coefficient depends linearly on the wave number, i.e.,

$$g = g_a \frac{\nu_0}{\nu_a}, \tag{9}$$

where $\nu_a = 997\ \mathrm{cm}^{-1}$ denotes the average value of the wave numbers of all measured QCLs. Figure 6 shows the calculated values of g (dots) for all experimentally investigated QCLs according to Eq. (5), where g has been obtained by adjusting the calculated threshold current density to the measured one. The dashed line indicates the wave-number-independent value of 7.2 $\mathrm{cm\,kA}^{-1}$, the solid line the dependence of the gain coefficient on the wave number according to Eq. (9). The calculated values of g for the different QCLs exhibit a large scatter between $g = 5$ and 10 $\mathrm{cm\,kA}^{-1}$. The increase of g with increasing ν_0 is due to the dependence of g on ν_0 as given by Eq. (9). Although a correlation between the gain coefficient and the injector doping density is not observed in Fig. 6, it cannot be ruled out. Our derived values for $g(\nu_0)$ are in the same range as the value of 8.7 $\mathrm{cm\,kA}^{-1}$ reported by Sirtori *et al.*[1] for a QCL with the same cascade structure, but using $Al_{0.9}Ga_{0.1}As$ WGs. However, for the same cascade structure, but with plasmon-assisted WGs, which actually should have no influence on the gain coefficient, values of $g = 14.2$, 15.8, and 13 $\mathrm{cm\,kA}^{-1}$ have been reported in Refs. 2 and 13. Theoretical models have predicted gain coefficients for GaAs-based QCLs of $g = 11.3\ \mathrm{cm\,kA}^{-1}$ in Ref. 15 and $g = 5.1\ \mathrm{cm\,kA}^{-1}$ in Refs. 16 and 17, where we have deduced this value from the maximum in the gain spectrum of Fig. 10 in Ref. 16 and from the threshold current density of Fig. 2 in Ref. 17. These literature data indicate a large variation of g, but our experimentally determined values are somewhat smaller than most values reported in the literature. For method I, a larger value of g would result in a increased value of $\alpha_{WG}(\nu_0)$ according to Eq. (7), which would be in better agreement with the literature data. At the same time, a larger value of g would result according to Eq. (5) in a decrease of the threshold current density j_{th}, which is in contrast to our measured data. Figure 4 shows that the trend of our measured $j_{th}(\nu_0)$ values is well described by our model. Furthermore, Table I also shows a good agreement between the measured and calculated values of j_{th} for the DLs and their corresponding reference QCLs. In particular, the larger calculated value of j_{th} for QCL1 with respect to that of DL1 has been experimentally verified. It can be explained within our model by the wave number dependence of the FCA and the difference in the lasing energies of QCL1 and DL1.

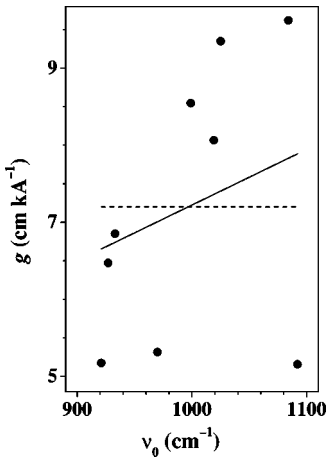

FIG. 6. Gain coefficient g vs ν_0 determined from the measured threshold current densities and calculated WG losses (dots). The dashed line indicates the wave-number-independent gain coefficient g_a obtained in Sec. V, the solid line describes the linear dependence of the gain coefficient on the wave number according to Eq. (9).

VIII. CONCLUSIONS

We have investigated the WG losses due to FCA and its influence on the threshold current density in GaAs/$Ga_{0.33}Al_{0.67}As$ QCLs with plasmon-assisted WGs as a function of the injector doping density. The QCLs nominally contain the same cascade structure except for the injector doping density, which influences the lasing wave number. We have determined the WG losses for the different QCLs in two ways. First, we used a model based on the in-plane component of the dielectric tensor to calculate the WG losses due to FCA. We find that the wave number dependence of the FCA in the WGs alone determines the decrease of the WG losses and subsequently the decrease of the threshold current density for our GaAs-based QCLs with increasing lasing energy. The influence of FCA in the cascade itself can be neglected except for very high injector doping densities. Second, we have directly measured the WG losses and threshold current densities on two-sectioned lasers and compared these values with our calculated results and values published in the literature. This comparison supports our analytical approach to determine the WG losses, providing a direct physical insight into the influence of FCA on the optical losses and the threshold current density. Finally, it offers a simple tool to estimate the WG losses without using a numerical solver.

ACKNOWLEDGMENT

This work was supported in part by the Deutsche Forschungsgemeinschaft within the framework of the Forschergruppe 394.

[1] C. Sirtori, P. Kruck, S. Barbieri, P. Collot, J. Nagle, M. Beck, J. Faist, and U. Oesterle, Appl. Phys. Lett. **73**, 3486 (1998).
[2] C. Sirtori, P. Kruck, S. Barbieri, H. Page, J. Nagle, M. Beck, J. Faist, and U. Oesterle, Appl. Phys. Lett. **75**, 3911 (1999).
[3] M. Giehler, R. Hey, H. Kostial, S. Cronenberg, T. Ohtsuka, L. Schrottke, and H. T. Grahn, Appl. Phys. Lett. **82**, 671 (2003).
[4] W. Walukiewicz, L. Lagowski, L. Jastrzebski, M. Lichtensteiger, and H. C. Gatos, J. Appl. Phys. **50**, 899 (1979).
[5] P. Kleinert and M. Giehler, Phys. Status Solidi B **136**, 763 (1986).
[6] E. Haga and H. Kimura, J. Phys. Soc. Jpn. **19**, 658 (1964).
[7] P. Pfeffer, I. Gorczyca, and W. Zawadzki, Solid State Commun. **51**, 179 (1984).
[8] R. T. Holm, J. W. Gibson, and E. D. Palik, J. Appl. Phys. **48**, 212 (1977).
[9] A. Kahan, AFCRL Research Report 63-325(II), 1963.
[10] V. M. Agranovich and V. E. Kravtsov, Solid State Commun. **55**, 85 (1985).
[11] H. Adamska and H. N. Spector, J. Appl. Phys. **56**, 1123 (1984).
[12] I. Vurgaftman and J. R. Meyer, Phys. Rev. B **60**, 14294 (1999).
[13] S. Barbieri, C. Sirtori, H. Page, M. Beck, J. Faist, and J. Nagle, IEEE J. Quantum Electron. **36**, 736 (2000).
[14] C. Gmachl, F. Capasso, D. L. Sivco, and A. Y. Cho, Rep. Prog. Phys. **64**, 1533 (2001).
[15] D. Indjin, P. Harrison, R. W. Kelsall, and Z. Ikonić, J. Appl. Phys. **91**, 9019 (2002).
[16] S.-C. Lee and A. Wacker, Phys. Rev. B **66**, 245314 (2002).
[17] S.-C. Lee, M. Giehler, R. Hey, T. Ohtsuka, A. Wacker, and H. T. Grahn, Semicond. Sci. Technol. **19**, S45 (2004).